Soft Matter

Cite this: *Soft Matter*, 2012, **8**, 8422

www.rsc.org/softmatter

PAPER

Colloidal particles at the interface between an isotropic liquid and a chiral liquid crystal

Anne C. Pawsey, Juho S. Lintuvuori, Tiffany A. Wood, Job H. J. Thijssen, Davide Marenduzzo and Paul S. Clegg*

Received 24th February 2012, Accepted 20th June 2012
DOI: 10.1039/c2sm25434d

We create an interface between a cholesteric liquid crystal (CLC) and an isotropic liquid (silicone oil) at which homeotropic anchoring leads to a well aligned cholesteric layer and the formation of the fingerprint texture. Fluorescent colloidal particles with planar surface anchoring are dispersed in the CLC and subsequently imaged using confocal microscopy. A majority of these particles decorate the interface between the CLC and the silicone oil. We present a detailed study of the position of the particles along the direction perpendicular to the interface: the final distribution of particles perpendicular to the interface has a clear dependence on the ratio between the particle size and the pitch of the CLC. This suggests, supported by simulations, that there is a particle size and pitch length dependent drive to expel particles, due to the elastic energy cost of remaining in the CLC. We use polarizing optical microscopy to observe changes to the fingerprint texture as the particles perturb the interface. This is combined with a qualitative study of the in-plane ordering of the particles. Chains of particles form perpendicular to the helical axis (parallel to the cholesteric layers), whereas disordered aggregates are seen where the direction of the helical axis is not uniform.

1 Introduction

Liquid crystals have partially ordered phases which can be perturbed by the addition of colloidal particles. The elastic energy of the liquid crystal adapts to accommodate the particles and this leads to novel particle–particle interactions. The resulting particle configurations include ordered arrays,[1] colloidal crystals,[2] and even amorphous glasses;[3] hence, this is a diverse and exciting class of materials. Fluid–fluid interfaces can also be used to template colloidal particle arrangements, producing well ordered two-dimensional crystals,[4] which can be extraordinarily sparse,[5] and also chains when the particles have rough surfaces.[6] Whilst the behaviour of particles trapped at fluid–fluid interfaces is relatively well understood, the behaviour when one of the phases is a partially ordered mesophase has only recently started to be explored and research so far has focused on nematic liquid crystals.[7,8]

We use a cholesteric liquid crystal (CLC) as a host; this mesophase possesses orientational order but additionally breaks translational symmetry. The average orientation of the molecules, denoted by the director, $\boldsymbol{n}$, maps out a helix along an axis, $\vec{h}$. The distance taken for the director to rotate through 2π gives the material an intrinsic length scale, the pitch length, p. Because the molecular orientation is periodic along the helix, its mathematical description is similar to that of a layered medium. The helical structure can be distorted in order to satisfy boundary conditions at a surface or in response to external fields or inclusions. The layers can either be distorted elastically where the layers bend smoothly or *via* the formation of defects.[9,10] The competition between the helical twist and surface anchoring of the liquid crystals leads to the appearance of striking cholesteric textures. Where the anchoring is homeotropic at both top and bottom surfaces the helical axis is forced to lie parallel to these surfaces and the fingerprint texture is observed. In this case the orientational order of the liquid crystal is frustrated because the constraints of both surface anchoring and helical twist cannot be satisfied simultaneously.[11] Cholesterics exhibit defects in the form of disclinations, where the orientational order is disrupted, and dislocations, where there is the insertion of an additional cholesteric layer. The latter are visible as the oily streaks in the planar texture and directly in the fingerprint texture.[11] The different defects can be described in terms of a "topological charge" which is the number of multiples of 2π that the director turns through when completing a circle counter-clockwise around the discontinuity.

Here we exploit the fingerprint texture so as to observe the response of the CLC to the additional boundary conditions imposed by micron-sized colloidal particles. There is a competition between the anchoring of the mesogens on the surface of the particle and the elastic distortion of the liquid crystal; a defect is created to balance these two effects.[12] The particle–particle interactions can then be mediated *via* both the elastic properties of the medium and the interactions of one or more defects

---

SUPA, School of Physics and Astronomy, University of Edinburgh, Mayfield Road, Edinburgh EH9 3JZ, UK. E-mail: paul.clegg@ed.ac.uk

(disclination lines can sometimes entangle more than one colloid). Colloids then self-assemble, for example, in a nematic as chains of particles.[1] The addition of twist in a cholesteric alters the defect structure.[13] For the case of planar anchoring of mesogens at the surface of the particles a pair of "Boojum" defects at the poles are expected in a nematic.[1,12] In a cholesteric these point defects open out into lines on the surface of the particle which twist with the helix. This complex physics increases the variety of aggregates formed: for $p < r$ particles aggregate in plates[14] and for $p > r$ tightly bound dimers are predicted.[15,16] However, even a small degree of twist can greatly increase the number of possible particle arrangements.[17] In some cases cholesteric "layers" are found to envelope the particle giving an object that resembles an "onion".[14] In order to clarify the effect of particles on the cholesteric liquid crystal it is useful to be able to observe the orientation of the helical axis. We use silicone oil which creates a fluid–fluid interface with the liquid crystal with strong homeotropic anchoring leading to a clear fingerprint texture as seen in Fig. 1(a) and (b).

The interface between a liquid and another medium is also a kind of defect. Colloidal particles can be found to sequester to this interface in a similar manner to the way they can occupy disclinations and dislocations. Colloids reduce the shared area between the two media leading, in cases where the Young equation holds (*i.e.* simple liquids, no complications due to elastic effects), to an energy saving $\Delta G = -\pi r^2 \gamma (1 \pm |\cos\theta|)^2$ where γ is the interfacial tension, θ is the contact angle of the colloid with the interface and r is the particle radius.[18] For pertinent values ($\approx$ 3.8 mN m^{-1}, 90°, 1.5 μm) the saving is $6.5 \times 10^7\ k_B T$ indicating that thermal fluctuations will be unable to free the particles from the interface. The aim here is to begin to understand how this trapping behaviour is modified when one of the liquids has liquid crystalline order.

In contrast to molecular surfactants, the colloids do not alter the interfacial tension between the liquids. Populations of colloids on fluid–fluid interfaces[4–6,18] self-organize due to standard colloidal interactions found in the bulk plus an interface specific capillary interaction.[19]

When one of the media is replaced by a complex fluid, such as a nematic liquid crystal, elastic effects, discussed above, come into play[20] leading to a larger range of colloidal patterns.[21–23] The type of structure produced depends on the liquid crystal film thickness, surface anchoring at the interface, and at the particles and the number density of colloids at the interface. The exact nature of the mechanisms involved are unclear, however, the additional interactions appear to be mediated by the liquid crystal elasticity and the formation of defects within the ordered phase. This is supported by the observation that chains of colloidal particles at a water–nematic interface can be triggered to change spacing and then form hexagonal crystals by the addition of a molecular surfactant.[24] This constituent is believed to modify the boundary conditions at the water–nematic interface which in turn changes the defects in the liquid crystal. Influence of the particles on the ordering of the liquid crystal itself has also been observed.[25]

In cholesterics the medium is spatially heterogeneous even before the addition of particles. Hence particles can occupy well defined locations within a well-ordered phase. Indeed, Mitov *et al.*[26] find that platinum nano-particles decorate the fingerprint texture of a long pitch cholesteric. With hybrid boundary conditions and gold nanoparticles Bitar *et al.* find a range of structures templated by the cholesteric texture which vary with film thickness.[27] The case of micron-sized particles at a CLC–isotropic liquid interface has not been explored.

We present a study of colloidal particles (diameter 1–10 μm) trapped at the interface between a cholesteric liquid crystal and an isotropic fluid (silicone oil). This system exhibits a number of new effects: first, there is a variation in the fraction of colloids found on the interface as a function of particle size and pitch length. This is ascribed to the elastic properties of the CLC: we use simulations to show that the elastic penalty varies with particle size and pitch length. Second, chain formation of colloids parallel to the helical layers is seen to be one mode of self assembly for this system. Finally isolated particles are seen to stabilize several different classes of defect.

2 Experimental techniques

2.1 Materials

The liquid crystal mixtures of nematic MDA-00-1444 ($n_e = 1.684$, $n_o = 1.507$) and chiral dopant MDA-00-1445 ($n_e = 1.67$, $n_o = 1.5$), both from Merck were mixed in the following ratios (by mass) 80 : 20 giving a pitch length of 1.5 μm and 90 : 10 giving a pitch length of 3.2 μm. The resultant mixtures were labelled with Nile Red (Aldrich); the low concentration used (0.01% by mass) ensures that the dye does not disrupt the liquid crystalline order. The colloidal particles were fluorescein isothiocyanate (FITC)-labelled melamine with carboxylate-modified surfaces (Fluka) with a range of diameters (1 μm, 3 μm, 6 μm, 10 μm). These were dried under vacuum at 40 °C overnight prior to use, then dispersed into the liquid crystal mixtures *via* a combination of stirring and sonication. It should be noted that all dispersions of melamine particles in CLC are stable in the bulk with macroscopic sedimentation only observed on a timescale of weeks. Small particles

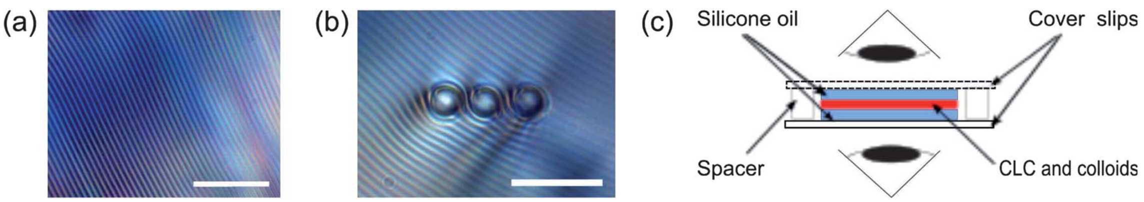

Fig. 1 (a) and (b) a pair of interfaces viewed through the overlying silicone oil. Scale bars 10 μm. (a) Unadorned fingerprint texture characterized by a reasonably uniform helical axis direction. (b) Polarising optical microscopy image of 3 μm colloids at the interface of a 1.5 μm pitch CLC. Cholesteric layers can be seen between the particles. (c) A schematic diagram of the experimental set up (not to scale, spacers are 50 μm). Samples have been studied from above and below.

are more difficult to disperse and required a longer duration of sonication. The volume fraction of colloids was 0.1% and the resultant mixtures are stable over the life time of the experiment.

To create a fluid interface with homeotropic anchoring, silicone oil (Aldrich) was spin coated onto a cover slip (Menzel Gläser) to give a uniform layer. Two types of sample were used, open and sealed cells. For the open cells, the oil coated slide was placed on the inverted microscope, a drop of liquid crystal was added followed by more silicone oil. The samples were then left to equilibrate prior to imaging for a minimum of 1 hour; they are quiescent after this time. For sealed cells, mylar spacers (50 μm) were attached to a microscope base slide (SN) using UV curing glue (Norland). Silicone oil was laid down between the spacers, a drop of LC added and a cover slip coated with oil placed on top. The edges of the cell were sealed with epoxy resin (Araldite) along the spacers and silicone vacuum grease (Dow Corning) along the open ends. Sealed cells were used on both upright and inverted microscopes, open cells were only used on inverted microscopes. A schematic of the sealed cells is shown in Fig. 1(c).

The CLC and the silicone oil are slightly miscible at room temperature. This alters the density of the CLC but, as the oil is not chiral, has no observable effect upon the pitch. The effect is temperature dependent; a phase diagram of a similar LC–silicone oil system can be found in ref. 28. We are well below the cholesteric–isotropic transition for our system and observe a stable interface both in the microscopy experiments and pendant drops.

2.2 Microscopy

Optical microscopy was carried out using an upright Nikon E800 microscope fitted with a QImaging Micropublisher 3.3 colour camera. All images were taken in transmission through crossed polarisers.

Confocal microscopy was performed using a Zeiss Observer.Z1 inverted microscope in conjunction with a Zeiss LSM 700 scanning system and a 63× 1.40 NA oil immersion objective. The Nile Red in the liquid crystal was excited with a 555 nm diode laser, the FITC in the colloids was excited using 488 nm diode laser. Transmission signals from both lasers were also recorded. A polarising filter aligned perpendicularly to the laser polarisation was placed in the light path for the transmission images. To increase the signal to noise ratio all images were averaged (4×).

2.3 Image analysis

Particle coordinates were found using particle tracking routines developed by E.R. Weeks and others[29] and were used to calculate distribution of the particle centres.

The analysis of the liquid crystal textures required the development of additional routines. The stripes were identified using the following processes implemented using LabVIEW Vision Assistant. The image was (where necessary) converted to grey scale and the contrast enhanced. The image was then thresholded to produce a binary image and eroded to give pixel wide stripes which correspond to the regions in the original image of maximum (minimum) intensity. The resulting stripes were then overlaid on the original image to aid defect identification.

For the analysis of the liquid crystal–oil interface, the mean image intensity per slice is plotted as a function of depth (slice number from confocal stack), the resulting profile is used to identify the location of the liquid crystal interface. Uncertainty in the vertical position of the particles relative to the interface ($\Delta z = \pm 0.3$ μm) is dominated by the effect of chromatic aberration.

2.4 Interfacial tension measurements

The interfacial tension of the liquid crystal–silicone oil interface, γ_{CS}, was measured using the pendant drop method with a Krüss EasyDrop tensiometer (model 65 FM40Mk2). CLC droplets of volume 31.3 ± 0.4 μL were suspended under silicone oil at 23 ± 1 °C. After 15 min of equilibration, digital snapshots were recorded from which values for γ_{CS} were extracted by fitting the Young–Laplace equation to the drop profile. Required input parameters for fitting include: the syringe needle diameter, 1.83 ± 0.01 mm, for pixel-size calibration and the density difference between the (silicone oil saturated) CLC and the silicone oil $\Delta\rho = 0.038 \pm 0.003$ g cm^{-3} (calculated by weighing known volumes of oil and saturated CLC). Three measurements on three different droplets were averaged to obtain the value of $\gamma_{CS} = 3.8 \pm 0.4$ mN m^{-1}. The error was calculated by combining the standard deviation of the three measurements with error estimates for temperature variations, density variations and the partial solubility of silicone oil in the CLC.[28] Given the complex nature of the CLC this measurement gives a bulk value which in practice may depend on the exact geometry of the experiment.

3 Results and discussion

The homeotropic anchoring at the oil–liquid crystal interface constrains the helical axis to lie in a plane perpendicular to the viewing (z) direction. The cholesteric layers are perpendicular to the oil interface and are visible as alternating bright and dark stripes when viewed between crossed polarisers. Dark (light) stripes correspond to places where the molecules are perpendicular (parallel) to the interface. The periodicity arises from the helical arrangement of the director: the distance between the centers of neighbouring stripes corresponds to a distance of a half pitch length. Fig. 1(a) shows a uniform fingerprint texture of the interface without colloids, with periodicity equal to a half of the pitch.

The addition of particles does not destroy the ordered phase, instead the direction of the helix is perturbed but the periodicity remains unchanged, Fig. 1(b). The experimental setup is presented schematically in Fig. 1(c). The melamine particles dispersed in CLC are sandwiched between two silicone oil layers.

Gravity plays a negligible role in our system: in the bulk sedimentation of colloids occurs only over a timescale of weeks. To show that it also plays a negligible role in the interfacial physics we investigate here, we evaluate the Bond number, $\mathrm{Bo} = \Delta\rho g r^2/\gamma_{CS}$, the ratio between the interfacial trapping force and the force due to gravity, where $\Delta\rho$ is the difference in density between the CLC and the melamine (150 Kg m^{-3}), r is the particle size (*e.g.* 3 μm) and γ_{CS} is the interfacial tension $\gamma_{CS} = 3.8 \pm 0.4$ mN m^{-1}. We find Bo ranges from 10^{-7} to 10^{-5} as we vary particle size indicating that the surface tension dominates over gravity and thus gravity should be unable to remove particles from, or indeed appreciably deform, the interface.

3.1 Particle distributions

The position of the particles with respect to the silicone oil–cholesteric interface was determined using fluorescence confocal microscopy. A majority of the particles are found on the interface between the oil (shown as black in Fig. 2(a) and (b)) and the liquid crystal (grey), colloids (green) can be seen on the interface and also in the case of 1 μm particles deep within the bulk liquid crystal. An example result of the image analysis is shown in Fig. 2(c): the smooth line indicates the intensity of the fluorescence from the Nile Red dye while the bars indicate the frequency of centre positions of the particles. The interface was taken to be the mid-point of this rise which was found to correspond well with the point at which the LC texture was first in focus but allowed for automation and comparison between different samples. Relative to this the vertical location of the particles with respect to the interface could be found. Particles which were within a distance of r + the confocal slice thickness (0.38 μm) were defined as being trapped at the interface (shaded (blue) region in Fig. 2(c)). It is important to note that while particles were found in the bulk of the liquid crystal (light (red) region) they were never found wholly within the silicone oil (white region).

Fig. 3(a) and (b) show the proportion of the particles found on the interface between the liquid crystal and the silicone oil (as opposed to the bulk of the LC) as a function of particle radius for two different pitch lengths of the cholesteric liquid crystal. A bigger proportion of large particles ($r > p$) are found on the interface than small ($r < p$) particles. Fig. 3(a) shows the proportion of particles on the interface as a function of radius/pitch length, more particles are found on the interface as this ratio increases.

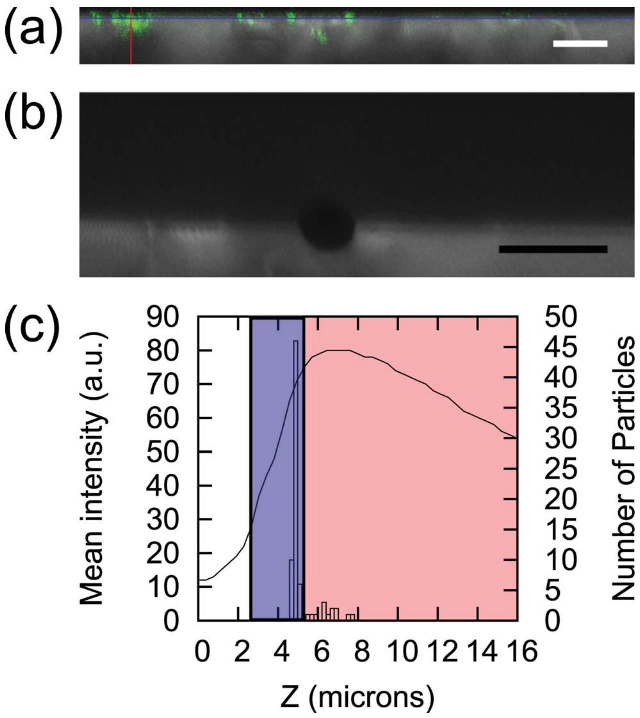

Fig. 2 (a) 1 μm particles at the interface (colloids green, liquid crystal grey). (b) A 10 μm particle at the interface of the liquid crystal (grey) colloid is black. Scale bars 20 μm. (c) Example graph of image intensity (line) and particle, r = 3 μm, positions (as histogram). Here the white region corresponds to silicone oil and the light (red) to CLC. The dark shaded (blue) region indicates the area where particles were considered to be trapped at the interface (see text for more details).

Further, it can be seen in Fig. 3(b) that the particles in 1.5 μm pitch CLC are preferentially expelled compared to those in 3.2 μm pitch CLC for the same radius. We associate this effect with changes to the liquid crystal elastic properties as a function of the helical pitch. The colloid induces a defect line in the cholesteric with a length that changes inversely with the pitch (see below); hence the defect is more energetically expensive at shorter pitch lengths.

The preferential expulsion of particles from the cholesteric liquid crystal, when ratio r/p increases is seen for both of the pitch lengths considered. The fact that not all particles, which were initially mixed into the CLC, are found on the interface (which is a deep energy minimum in view of the large proportion of the particles sequestered there) indicates that the system reaches a metastable state, with the proportion of particles at the interface unchanged over the lifetime of the experiment (days with closed cells, hours with open ones). This view is confirmed by additional experiments, when particles are mixed initially into the silicone oil. In this case, particles are found in steady state *only* on the interface, and never stuck in the oil phase.

These observations suggest that there is a particle size dependent force which drives particles to the interface, with larger particles being preferentially expelled. As the particles are found to be expelled to both upper and lower interfaces, with approximately equal probabilities when sandwiched between the silicone oil layers, gravity cannot provide the necessary driving force. In addition, in recent experiments[14] on the bulk system no sedimentation was observed over a time period of a year indicating that any dynamics due to gravity must be extremely slow. Close to the interface, dynamics may be further arrested by the appearance of an elastic barrier which has been predicted for a colloidal particle approaching an aligning surface in a nematic LC.[30]

A good candidate to expel the particles to the interface comes from the elastic cost associated with a particle with planar surface anchoring trapped in the bulk of a CLC. The Boojum defects seen in the nematic expand to become disclinations in the CLC (shown schematically in Fig. 4).[13]

To evaluate the elastic cost of having a colloidal particle with a finite surface anchoring, W, embedded into bulk cholesteric liquid crystal characterised by a pitch length p and elastic constant K, we performed simulations using a Landau-de Gennes free energy model for chiral liquid crystals[11,31] (in the absence of flow). The simulations were carried out in a cubic (periodic) box of volume $(4p)^3$ imposing planar alignment of the liquid crystal director at the particle surface with finite surface anchoring strength ($Wr/K > 1$).† The elastic penalty can be estimated as $\Delta U = F_W - F_{W=0}$, where F is the minimised free energy of the system (including the surface anchoring) and $F_{W=0}$ refers to a system with non-interacting colloidal particle with the

---

† In simulations $W = 32K/p$. For more details of the method see refs. 13, 16 and 33 (the liquid crystal parameters are the same as in ref. 13).

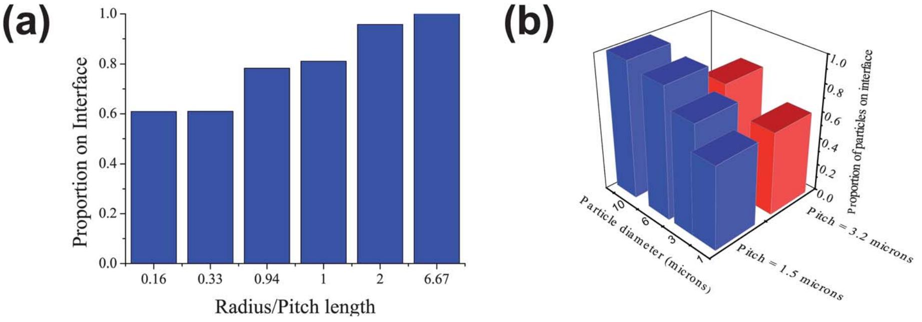

Fig. 3 (a) Proportion of particles on the interface as a function of radius/pitch length. (b) Proportion of particles found on the interface as a function of pitch length and particle size.

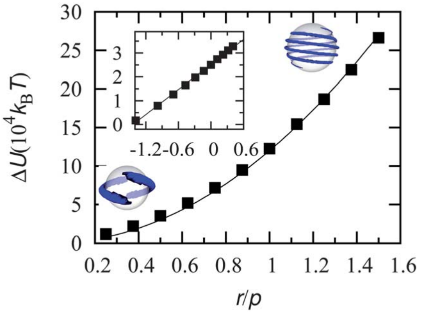

Fig. 4 Showing the elastic energy cost, ΔU, determined by simulating a colloidal particle, radius r, with planar surface anchoring submerged in a cholesteric liquid crystal, pitch p schematics show the defect structures around particles as discussed in the text. Inset: a log–log plot of the same values. The solid lines are a functional form described in the text.

same size, r. Fig. 4 shows an estimated ΔU for variable r and constant p, together with a fit to $\Delta U = a(r/p)^2$, with a a positive constant with the units of energy. The inset shows the same data on a log–log plot. Here the fit is $\ln(\Delta U) \approx n\ln(r/p) + a'$, with $n \approx 1.75 \pm 0.03$. The simulation data are therefore compatible with an energetic cost $\Delta U \sim Kr^2/p$, which contrasts with the nematic limit, where dimensional analysis suggests $\Delta U \sim Kr$.

The higher power in r found in the scaling of the free energy cost with respect to the nematic limit can be intuitively explained; larger particles create longer defects which cost additional energy and provide a drive to expel the particles to the interface. This is in contrast to the nematic case where the Boojum defects are independent of the particle radius. Importantly, this elastic cost leads, by dimensional analysis, to an elastic force $\sim Kr/p$, which increases with the ratio r/p. This provides an explanation for the experimental findings of Fig. 3 that the proportion of colloidal particles at the interface increase when ratio r/p is increased.

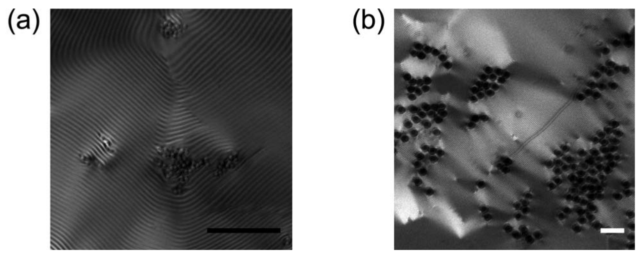

Fig. 5 (a) A transmission image from the 555 nm laser with crossed polarisers of a 1 μm particles at the interface of a $p = 1.5$ μm CLC. (b) Fluorescent confocal image of a $p = 1.5$ μm CLC only, 3 μm colloids appear black. Scale bar 10 μm.

3.2 Particle aggregates

In our sample cells the direction of the helical axis within the xy plane can vary; we can easily observe this variation and its influence on the distribution of particles. This is in contrast to experiments performed with bulk cholesteric where the helical axis is forced to lie parallel to the viewing direction.[14] Fig. 5 shows the variation in cholesteric texture and the resulting arrangements of particles. Particles are found singly, in chain-like aggregates and in amorphous "clumps". Aggregates form where the helical axis changes direction. This could be due to expulsion of the particles from the ordered cholesteric to zones of high defect density as the system equilibrates; images are taken once the cholesteric texture is static. Due to the high viscosity of the samples Brownian motion is not observed and particle distributions appear quiescent. All aggregate types are observed for all particle sizes and pitch lengths.

Some deformation of the helical axis is required in order to accommodate the surface anchoring at the colloids. The lowest energy configurations could well be the chain-like aggregates, Fig. 6, which involve relatively little perturbation of the direction of the helical axis. In the bulk only plate-like aggregates perpendicular to the helical axis are observed.[14] It is tempting to say that the chains correspond to the edges of these plates, found perpendicular to the helical axis where the direction of the axis is reasonably uniform. However, the chains we observe are lines along the interface and do not propagate deep into the sample as they would if they represented a slice through a plate.

In between the particles the surface anchoring conditions and the helical axis direction cannot both be satisfied. The direction of the helix becomes distorted to allow the surface anchoring to be maintained. For particles larger than the pitch length the particles do not touch within the chains Fig. 1(b), 6(a) and (b). The spacing is roughly the period of the stripes, suggesting that there may be cholesteric layers wrapping the particles as with previous observations of "onions".[14]

The 1 μm particles, Fig. 6(c), touch within the chains which can be seen to follow the fingerprint stripes. The chains of small particles are found in the bright stripes where the helix imposes

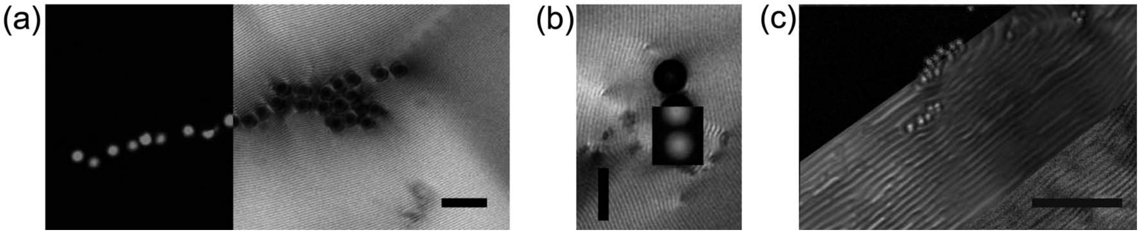

Fig. 6 Confocal images of particles at the LC interface. Particle centres found using particle tracking routines and distances calculated. (a) 3 μm particles at the interface of a 1.5 μm pitch CLC confocal image. The right hand side is the fluorescent signal from the CLC showing the arrangement of the cholesteric layers. The left hand side shows the fluorescent signal from the colloids. Average inter-particle spacing (centre to centre) 3.44 μm (*i.e.* 0.44 μm + diameter) (b) 6 μm particles at the interface of a 1.5 μm pitch CLC, fluorescent signal from the CLC showing the arrangement of the cholesteric layers, the overlay shows the confocal fluorescent signal from the colloids. Inter-particle spacing (centre to centre) 6.56 μm (*i.e.* 0.5 μm + diameter), (c) 1 μm particles at the interface of a 1.5 μm pitch length CLC. Confocal image: top section signal from the colloids, centre section transmission signal, bottom section fluorescent signal from CLC. The particles are touching. Scale bars 10 μm. All textures observed through the transparent silicone oil layer.

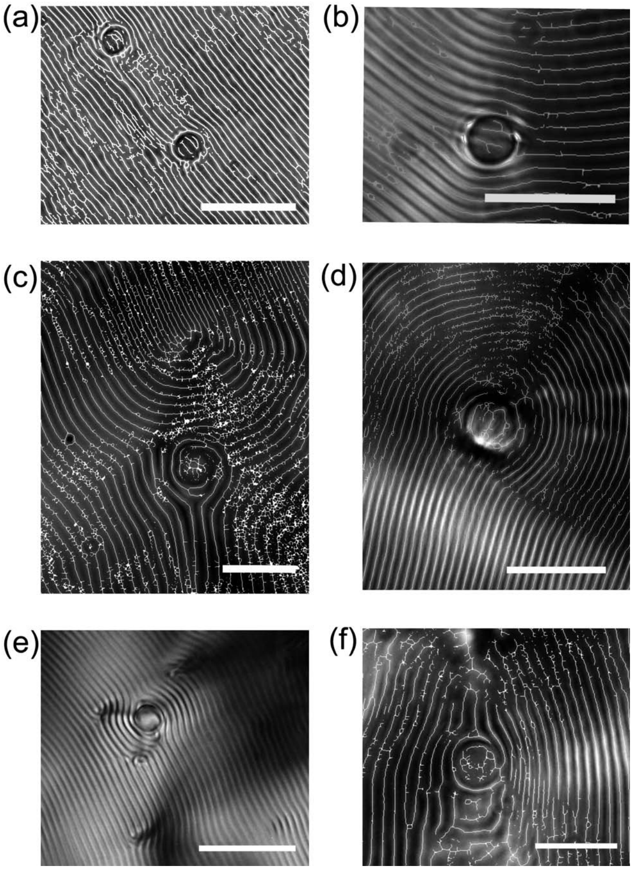

Fig. 7 Polarising optical microscopy images of single particles showing the influence of particles on the cholesteric layers. Bright lines denoting pixels with local maximum intensity added to guide the eye. Scales bars (a, d, e) 10 μm (b, c, f) 5 μm. (a) 3 μm particles in 1.5 μm pitch CLC; (b) 3 μm particle in 1.5 μm pitch CLC; (c) 6 μm particle in 1.5 μm pitch CLC; (d) 3 μm particle in 1.5 μm pitch CLC; (e) 3 μm particle in 1.5 μm pitch and (f) 3 μm particle in 1.5 μm pitch CLC.

that the mesogens lie parallel to the interface frustrating the homeotropic alignment imposed by the interface. This produces a favourable location, *i.e.* a template, for the small colloids to sit in chains.[32] Particles do not touch when found close to each other but in adjacent stripes.

3.3 Single particles

Fig. 7 shows the arrangement of the cholesteric layers around single particles. We identify three distinct cases. In the first, Fig. 7(a) and (b), the layer spacing, direction and alignment are relatively unperturbed by the presence of the particle and no obvious defects are seen. This is likely to be the lowest energy state and corresponds to that found in simulations.[32] In the computational studies a defect, in the form of a Boojum expanded into a line, is formed which, for us, could be unresolvably close to the particle surface.

In the second case Fig. 7(c) and (d), the particles are associated with a chi edge defect. This defect separates regions with differing numbers of layers (*i.e.* additional cholesteric layers are introduced). Chi edge defects are postulated to be the structure of the oily streaks found in the Grandjean (planar) texture of the cholesteric. The association of colloids with oily streaks, leading to the stabilisation of the oily streak network has been reported[34] so it is unsurprising that colloids are found in analogous regions here. The formation of defects costs energy due to the formation of a disordered core: in the bulk case it has been postulated that the particle takes out this high energy region pinning the defect in place. A similar mechanism is likely to be in play here leading to the colloids stabilizing the defect.

We also find defects spatially separated from the particles, Fig. 7(e). Here the external defect may represent the topological charge required to balance that of the defect created at the particle. Other more complicated cases are also observed, Fig. 7(f). It is possible that these spatially extended arrangements of defects are metastable in comparison to more compact configurations. We find these defect structures for all particle sizes and pitch lengths. It is possible that the wide variety of defect structures encountered leads to the variety in particle aggregate size and shape.

4 Conclusion

We have studied a cholesteric liquid crystal–silicone oil interface decorated with particles. The final distribution of particles perpendicular to the interface has a significant dependence on the ratio between their size and the pitch length. Using simulations we establish that the elastic energy penalty of a colloid in the bulk of the CLC scales as Kr^2/p, leading to a force $\sim Kr/p$ which suggests that this is the cause of large particles being preferentially expelled. The arrangement of particles in the plane of the interface is also size dependent: when the particles are smaller than the pitch connected chains are found. For larger particles the cholesteric layers wrap the particles in a manner suggestive of the "onions" in ref. 14 leading to a separation of particles within chains. These chains form perpendicular to the helical axis (parallel to the cholesteric layers). Disordered aggregates are seen where the direction of the helical axis is not uniform. The association of single particles with at least three different defect types suggests a mechanism for this disorder.

Acknowledgements

This work was funded by EPSRC Grant no. EP/E030173 and no. EP/I030298. A.C.P. gratefully acknowledges the support of the EPSRC Scottish Doctoral Training Centre in Condensed Matter Physics.

References

1 P. Poulin and D. A. Weitz, *Phys. Rev. E: Stat. Phys., Plasmas, Fluids, Relat. Interdiscip. Top.*, 1998, **57**, 626.
2 M. Ravnik, *Soft Matter*, 2009, **5**, 269.
3 T. A. Wood, J. S. Lintuvuori, A. B. Schofield, D. Marenduzzo and W. C. K. Poon, *Science*, 2011, **334**, 79.
4 P. Pieranski, *Phys. Rev. Lett.*, 1980, **45**, 569.
5 T. S. Horozov, R. Aveyard, J. H. Clint and B. P. Binks, *Langmuir*, 2003, **19**, 2822.
6 D. Stamou, C. Duschl and D. Johannsmann, *Phys. Rev. E: Stat. Phys., Plasmas, Fluids, Relat. Interdiscip. Top.*, 2000, **62**, 5263.
7 Y. Bai and N. L. Abbott, *Langmuir*, 2011, **27**, 5719.
8 M. Tasinkevych and D. Adrienko, *Condens. Matter Phys.*, 2010, **13**, 1.
9 T. Lubensky, *Phys. Rev. A: At., Mol., Opt. Phys.*, 1972, **6**, 452.
10 I. Smalyukh and O. Lavrentovich, *Phys. Rev. E: Stat., Nonlinear, Soft Matter Phys.*, 2002, **66**, 051703.
11 P. G. de Gennes and J. Prost, *The Physics of Liquid Crystals*, OUP, 1993.
12 H. Stark, *Phys. Rep.*, 2001, **351**, 387.
13 J. S. Lintuvuori, K. Stratford, M. E. Cates and D. Marenduzzo, *Phys. Rev. Lett.*, 2010, **105**, 178302.
14 N. Hijnen, T. A. Wood, D. Wilson and P. S. Clegg, *Langmuir*, 2010, **26**, 13502.
15 F. E. Mackay and C. Denniston, *Europhys. Lett.*, 2011, **94**, 66003.
16 J. S. Lintuvuori, K. Stratford, M. Cates and D. Marenduzzo, *Phys. Rev. Lett.*, 2011, **107**, 267802.
17 U. Tkalec, M. Ravnik, S. Copar, S. Zumer and I. Musevic, *Science*, 2011, **333**, 62.
18 B. P. Binks and T. S. Horozov, *Colloidal Particles at Liquid Interfaces*, Cambridge University Press, 2006.
19 M. Oettel and S. Dietrich, *Langmuir*, 2008, **24**, 1425.
20 M. Oettel, A. Domnguez, M. Tasinkevych and S. Dietrich, *Eur. Phys. J. E*, 2009, **28**, 99.
21 A. Nych, U. Ognysta, V. Pergamenshchik, B. Lev, V. Nazarenko, I. Musevic, M. Skarabot and O. Lavrentovich, *Phys. Rev. Lett.*, 2007, **98**, 057801.
22 M. A. Gharbi, M. Nobili, M. In, G. Prevot, P. Galatola, J.-B. Fournier and C. Blanc, *Soft Matter*, 2011, **7**, 1467.
23 I. Smalyukh, S. Chernyshuk, B. Lev, A. Nych, U. Ognysta, V. Nazarenko and O. Lavrentovich, *Phys. Rev. Lett.*, 2004, **93**, 117801.
24 G. M. Koenig, I.-H. Lin and N. L. Abbott, *Proc. Natl. Acad. Sci. U. S. A.*, 2010, **107**, 3998.
25 I.-H. Lin, G. M. Koenig, J. J. de Pablo and N. L. Abbott, *J. Phys. Chem. B*, 2008, **112**, 16552.
26 M. Mitov, C. Portet, C. Bourgerette, E. Snoeck and M. Verelst, *Nat. Mater.*, 2002, **1**, 229.
27 R. Bitar, G. Agez and M. Mitov, *Soft Matter*, 2011, **7**, 8198.
28 J. C. Loudet, P. Barois, P. Auroy, P. Keller, H. Richard and P. Poulin, *Langmuir*, 2004, **20**, 11336.
29 R. Besseling, L. Isa, E. R. Weeks and W. C. K. Poon, *Adv. Colloid Interface Sci.*, 2009, **146**, 1.
30 D. Cheung and M. Allen, *Phys. Rev. E: Stat., Nonlinear, Soft Matter Phys.*, 2007, **76**, 041706.
31 A. N. Beris and B. J. Edwards, *Thermodynamics of Flowing Systems*, Oxford University Press, Oxford, 1994.
32 J. S. Lintuvuori, A. C. Pawsey, P. S. Clegg and D. Marenduzzo, in preparation.
33 J. S. Lintuvuori, D. Marenduzzo, K. Stratford and M. E. Cates, *J. Mater. Chem.*, 2010, **20**, 10547.
34 M. Zapotocky, L. Ramos, P. Poulin, T. C. Lubensky and D. A. Weitz, *Science*, 1999, **283**, 209.